frontiers | Frontiers in Remote Sensing

TYPE Original Research
PUBLISHED 22 January 2025
DOI 10.3389/frsen.2024.1459524

OPEN ACCESS

EDITED BY
Saeedeh Eskandari,
Research Institute of Forests and Rangelands, Iran

REVIEWED BY
Qin Ma,
Nanjing Normal University, China
Yuanhui Zhu,
Arizona State University, United States

*CORRESPONDENCE
Samuel Favrichon,
samuel.favrichon@gmail.com

RECEIVED 04 July 2024
ACCEPTED 23 December 2024
PUBLISHED 22 January 2025

CITATION
Favrichon S, Lee J, Yang Y, Dalagnol R, Wagner F, Sagang LB and Saatchi S (2025) Monitoring changes of forest height in California.
Front. Remote Sens. 5:1459524.
doi: 10.3389/frsen.2024.1459524

Monitoring changes of forest height in California

Samuel Favrichon[1]*, Jake Lee[1], Yan Yang[1,2], Ricardo Dalagnol[2,3], Fabien Wagner[2], Le Bienfaiteur Sagang[2,3] and Sassan Saatchi[1,2,3]

[1]Jet Propulsion Laboratory, California Institute of Technology, Pasadena, CA, United States, [2]Ctrees, Pasadena, CA, United States, [3]Center for Tropical Research, Institute of the Environment and Sustainability, University of California Los Angeles, Los Angeles, CA, United States

Forests of California are undergoing large-scale disturbances from wildfire and tree mortality, caused by frequent droughts, insect infestations, and human activities. Mapping and monitoring the structure of these forests at high spatial resolution provides the necessary data to better manage forest health, mitigate wildfire risks, and improve carbon sequestration. Here, we use LiDAR measurements of top of canopy height metric (RH98) from NASA's Global Ecosystem Dynamics Investigation (GEDI) mission to map vegetation height across the entire California for two different time periods (2019–2020 and 2021–2022) and explore the impact of disturbance. Exploring the reliability of machine learning methods for temporal monitoring of forest is still a developing field. We train a deep neural network to predict forest height metrics at 10-m resolution from radar and optical satellite imagery. Model validation against independent airborne LiDAR data showed a $R^2 \geq 0.65$ for the top of canopy height outperforming existing GEDI-based height maps and with improved sensitivity for mapping tall trees (RH98 $\geq$ 50 m) across California. Height showed distinct spatial variations across forest types offering quantitative and spatial information to evaluate forest conditions. The model, trained on data from 2019 to 2020, showed a similar accuracy when applied to satellite imagery acquired in 2021–2022 allowing a robust detection of changes caused by natural and man-made disturbances of forest. Changes of height captured impacts of tree mortality and fire intensity, pointing to the influence of wildfire across landscapes. Fires caused more than 60% of the large forest disturbances between the two time periods. This study demonstrates the benefits of using locally trained ML models to rapidly modernize forest management techniques in the age of increasing climate risks.

KEYWORDS

forest height, remote sensing, machine learning, California, wildfire, change detection, GEDI

1 Introduction

The contribution of forestland to emissions offset in the United States has remained relatively stable since 2005 despite steady declines in economy-wide CO2 emissions over that period (Domke et al., 2020). This suggests that the forest carbon sink in the United States, which is driven in large part by forest regrowth following harvest and natural disturbances, is slowly diminishing (Williams et al., 2016; Pugh et al., 2019; Quirion et al., 2021). This threat to the US forest sink is especially significant in California, and the Pacific Northwest where frequent droughts have caused increasingly intense wildfires and insect infestation, reducing the forest carbon stocks and productivity in the last two decades

(Yu et al., 2022; Coffield et al., 2022). A history of fire suppression due to forest management has increased fuel stocks and altered fire regimes, causing catastrophic fires under cascading effects of climate change (Keane, 2002). The changes of forest carbon and health have devastating implications for California's emission reduction strategy and threatens its future economy by directly impacting landowners, corporations, and communities living near and in forests (Badgley et al., 2022).

One of the challenges associated with understanding the threat to California forests and its inhabitants is the lack of detailed, accurate, and frequent information on changes of forest height (and the associated fuel load, and the carbon density) at the state level. Surveys of forests across California over the last century (1930s–2000s) show a significant demographic shift in forest height accompanied by a shift in composition toward increased dominance by oaks relative to pines (McIntyre et al., 2015; Hill and Field, 2021). In recent years (1990s), these surveys are performed every 10 years in a network of forest inventory and analysis (FIA) plots. However, the small number of FIA plots (about 5,300 1-acre plots) sampling more than 32 million acres of forests in California and collected over a decade, is not enough to capture widespread tree mortality and frequent disturbance that alters forest height and biomass rapidly (Yu et al., 2022). Therefore, there is an urgent need to map and frequently monitor spatial variations of forest height at the scale of disturbance and management activities across California. Widespread mapping of vegetation structure and above ground biomass at local, regional, and global scales have become possible by using airborne and space borne LiDAR (Light Detection and Ranging) sensors from the beginning of this century (Dubayah and Drake, 2000; Næsset, 2002; Lim and Treitz, 2004; Lefsky, 2010; Saatchi et al., 2011; Bruening et al., 2023). Modern LiDAR sensors measure the timing and intensity of reflected energy from forest attributes, providing relatively continuous waveforms related to the vertical distribution of plant material (branches and leaves) and accurate information on forest height and terrain elevation (Eitel et al., 2016; Dong and Chen, 2017; Kellner et al., 2019). In recent years, the applications of LiDAR have broadened in forest ecology by quantifying 3D structure, demography, and gap dynamics (Vepakomma et al., 2008; Kellner and Asner, 2009; Ferraz et al., 2016; Dalagnol et al., 2021; Jucker, 2022), carbon stocks and dynamics (Asner and Mascaro, 2014; Stark et al., 2012; Moura et al., 2020; Meyer et al., 2013), and forest disturbances (Wulder et al., 2008; García et al., 2017; Jeronimo et al., 2018).

In California, LiDAR measurements have been used to quantify structure and fuels over some of the tallest, and most complex landscapes in the world (Kelly et al., 2017; Tang et al., 2014; Su et al., 2017). Estimation of forest fuels, the organic matter available for fire ignition and combustion, are considered the most essential attributes of California forests and the key component of fire management activities (Keane et al., 2004). The fuel loads are directly linked to measurements of forest height and biomass and can be estimated from ground over small areas and from remote sensing measurements across larger landscapes (Anderson et al., 2005; Saatchi et al., 2007; Skowronski et al., 2011; Kramer et al., 2016; Garcia et al., 2017).

Although widespread airborne LiDAR data are now available over California, the measurements are acquired over multiple years with different sensor characteristics, limiting their use for the monitoring of forest height across the state. Optical and radar remote sensing observations from space may provide a reliable alternative for mapping and monitoring forest height over large areas. They can be combined with NASA's Global Ecosystem Dynamics Investigation (GEDI) that collected LiDAR samples globally between 2019 and 2023. It provides billions of waveform observations (~4% of the Earth surface) across global forests (Dubayah et al., 2020). Data from GEDI have already been used as reference for vegetation height to develop global vegetation height maps at 10 and 30 m resolutions (Potapov et al., 2021; Lang et al., 2022). However, these maps, although excellent for continental and global studies of ecosystems, may have large uncertainty for local studies and forest management applications. For example, the two aforementioned products show little sensitivity to tall trees of California ($\geq$50 m) and have large uncertainty when compared to local airborne LiDAR measurements (RMSE $\geq$ 12 m, $R^2 \leq 0.6$). These are likely due to the global-scale machine learning training, which cannot capture local forest height variations accurately. Local maps have been shown to improve the accuracy compared to the global products, providing better estimates of the fine scale vegetation heights (Schwartz et al., 2023; Fayad et al., 2024). A second aspect not yet addressed in methodologies developed to estimate vegetation height (or biomass) from remote sensing observations is the reliability over time. Improving the accuracy of models and still being able to generalize to different observation conditions has not yet been explored.

Here, we want to evaluate the capacity of machine learning based model to monitor forest height changes in California. We develop a model to map forest height over the entire California, reducing the uncertainty in spatial variations compared to global maps, and improving estimation of tall forests $\geq$ 50 m. The model is then applied to two different time periods to enable an estimation of changes of vegetation height with time. These are critical contributions to state-wide forest carbon management wildfire mitigation activities and ecosystem health and diversity (Hakkenberg et al., 2023; LaRue et al., 2023; Vogeler et al., 2023). Using satellite imagery from optical and radar sensors and surface topography, we map the variations of vegetation height as measured by GEDI LiDAR waveform across the state. The estimation is performed using a deep-learning model utilizing GEDI sample data for training and the spatial variations of the high-resolution data from the remote sensing predictors as independent variables. The accuracy of the derived maps is estimated against independent airborne LiDAR campaigns available across the state, and the changes occurring over California are evaluated in comparison with existing products of forest degradation as well as coarse scale changes of height estimated from GEDI.

The first sections of this paper describe the different datasets used, and the methodologies developed to achieve the objectives. A summary of the different steps of the analysis is provided in Supplementary Figure S6. The results provide an analysis of the output maps, compared to reference data, and as a tool for change monitoring at high resolution. Finally, a discussion of the limitation of such remote sensing derived vegetation height maps is provided.

2 Data and methods

2.1 GEDI waveform data

The Global Ecosystem Dynamics Investigation (GEDI) is a LiDAR mission launched in 2018 onboard the International Space Station (ISS). The waveforms are sampled along ISS orbital tracks and from different laser beams to measure waveforms returns. The variations of vegetation structure and the biomass (Dubayah et al., 2020) can then be inferred from the waveform. Since the beginning of science data collection in 2019, GEDI has been providing waveforms at approximately 25 m footprints across the Earth between ±53° latitude. The measurements obtained by GEDI are sparsely distributed along the orbits of the ISS, without a repeated observation pattern nor a really random sampling. The LiDAR pulse returned waveform is recorded every 60 m along the track, with 600 m separating the individual laser beams. We only consider nighttime measurements recorded during the growing season (April to October) to avoid phenological changes and limit snow cover effect across California. The waveforms are all originating from full power beams with a sensitivity above 0.9, and possessing valid degradation and quality flags. We use the Level 2A products and the waveform return percentiles, referred to as relative heights, the 98th percentile (RH98) representing the maximum height of vegetation. To increase the available number of observed heights from GEDI we aggregate data from two time periods 2019–2020 and 2021–2022 to be used in this study. In order to achieve a similar resolution, all datasets are resampled with a nearest neighbor method to the Sentinel-2 10 m pixel resolution, over California.

2.2 Airborne LiDAR data

Airborne Laser Scanning (ALS) data with contiguous coverage of different areas of California forests was used to validate the accuracy and spatial variations of vegetation structure of the maps created using the GEDI samples and our model. The ALS observations come from multiple sources. Three field sites within the Sierra Nevada region, Lower Teakettle (TEAK), Soaproot Saddle (SOAP), and San Joaquin Experimental Range (SJER) that are acquired as part of the National Ecological Observatory Network (NEON) funded by the National Science Foundation (NSF) (Schimel et al., 2007; National Ecological Observatory Network, 2023). The sites were surveyed during the leaf-on season in 2019 across a variety of elevations and forest types, with TEAK and SOAP sites surveyed in June and SJER surveyed in March for a total area of approximately 70 km^2. The average point density of the ALS point clouds was ~6 points per square meter. The point clouds were filtered for noise using the *Statistical Outliers Removal* function and the 98 percentiles of the LiDAR returns in a 10 × 10 m regular grid is extracted for comparison with our model estimates (Roussel et al., 2020). In addition to the NEON sites, 39 sites from the United States Geological Survey (USGS) LiDAR data collected between 2018 and 2020 across different vegetation covers, covering ~200 km^2 were used for validation. Canopy Height Models (CHM) at 1 m spatial resolution were collected and the maximum value within each 10 m pixel computed for comparison with the mapped RH98 values. The distribution of the validation sites is apparent on Supplementary Figure S1.

2.3 Remote sensing data

Three distinct satellite data sources are used as input to the model to predict vegetation height metrics. For optical imagery, we use Sentinel-2 imagery in the visible and infrared bands (Drusch et al., 2012). We specifically use the blue, green, red, and near-infrared bands at their native 10 m spatial resolution. A mosaic was created by taking the median values from cloud-free images captured between April and October for the years 2019–2020 and 2021–2022 over California. The second source is data from the Advanced Land Observation Satellite (ALOS-2), operated by the Japanese space agency, carrying an L-band synthetic aperture radar PALSAR 2 (Rosenqvist et al., 2007). Both polarization (HH, HV) measurements are provided in a mosaic with 25 m resolution for each year. The lower frequency of L-band measurements allows for penetration through the canopy cover, providing complementary information to the visible and infrared observations (Shimada et al., 2014). To match the time periods used from the GEDI measurement, the mean of the 2019 and 2020 mosaics is used to represent the 2019–2020 period, and the 2021 imagery only to represent the 2021–2022 period, as data for 2022 are not available from JAXA yet. The third dataset is the Copernicus digital elevation model (DEM) GLO-30 dataset (Fahrland et al., 2020). Elevation plays a significant role in determining the distribution of vegetation structure and types in California. It is a well-known factor influencing plant traits, and the correlation between tree cover and elevation profiles has been extensively described in previous studies (Critchfield, 1971; Rybansky et al., 2016). Additionally, elevation is crucial in analyzing the impact of topography on LiDAR returns (Khalefa et al., 2013). Wall-to-wall mosaics of these datasets were prepared over California at 10 m spatial resolution for the two analyzed different time periods considered using the Google Earth Engine platform (Gorelick et al., 2017).

2.4 Ancillary data

We selected a set of ancillary datasets for data analysis and validation of vegetation structure maps. The datasets are produced by the California Department of Forestry and Fire Protection (CALFire) in order to facilitate research and forest management across the state. We downloaded the map of Wildlife Habitat Relationship classes (WHRTYPE) from (Mayer and Laudenslayer, 1988; CALVEG and California Wildlife Habitat Relationship, 2022), which represents a comprehensive land cover map with more than 50 vegetation classes for the entire state of California. We also used the extents of recent large fires (≥5000 acres) that occurred between 2019 and 2022 in California (CALFIRE, 2023) in order to study changes of forest height across landscapes in burned areas. To complement the fire extents, the Monitoring Trends in Burn Severity (MTBS) program (Finco et al., 2012), provides a map describing the burn severity within each fire, from unburned to high severity (1–4), and areas with increased post-fire greenness (5).

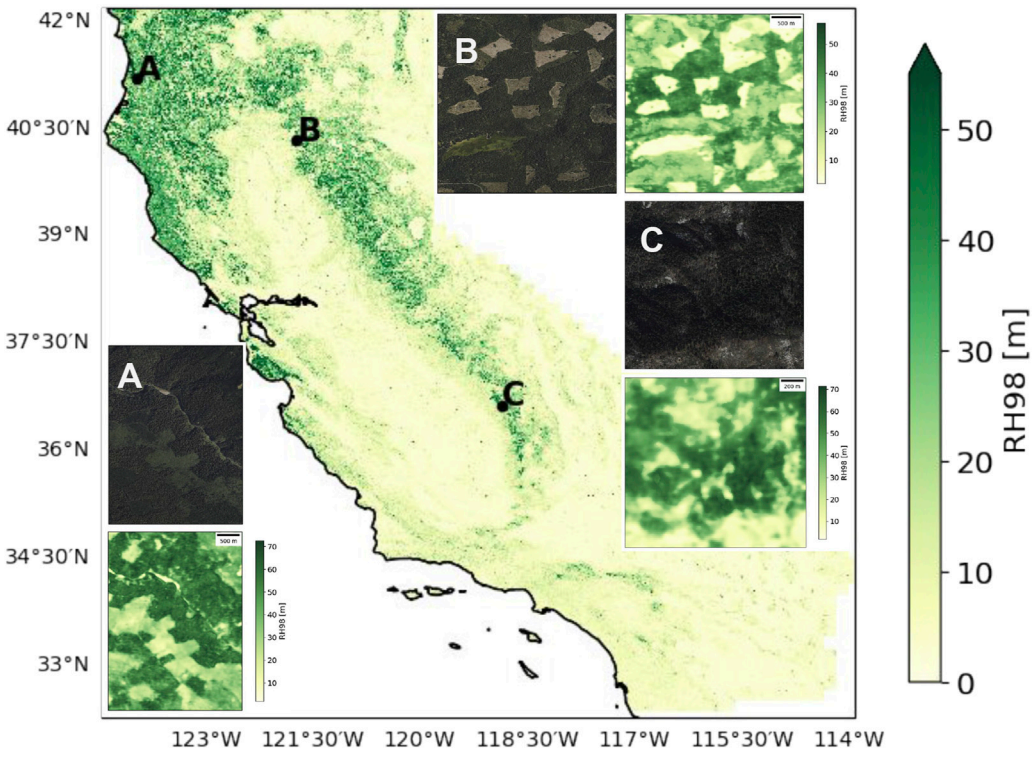

FIGURE 1
Map of the top canopy height (RH98) of California forests for the period 2019–2020. The three insets **(A–C)** show a zoom-in of selected sites with RGB satellite imagery from Bing© alongside predicted heights from our model.

Additionally, the California Department of Water Resources (DWR) has created watershed maps, which are manageable units of land with geographic coherence, averaging around 3 km^2. These watershed maps are utilized to aggregate high-resolution data and allow for comparison with aggregated sparse data. The shapes of the watersheds can be obtained from the Relative Watershed Condition dataset (The Cadmus Group, Inc., 2013).

Finally, existing height maps from (Potapov et al., 2021; Lang et al., 2022) were obtained for inter comparison of the height maps. These maps are available at similar resolution from 10 to 30 m and also used LiDAR data from space borne or airborne sensors to train machine learning models relying on different combinations of input data.

2.5 Model implementation

We employ a deep learning model to establish the relationship between the remote sensing predictor variables and the sparsely distributed relative height metrics derived from GEDI waveform measurements. The predictors consist of seven layers: four bands from Sentinel-2 data, two bands from the ALOS2 L-band backscatter, and one band from the GLO-30 digital elevation model. Our method adopts an encoder-decoder architecture similar to the U-Net network (Ronneberger et al., 2015), using an EfficientNet encoder (Tan and Le, 2021), that has demonstrated promising performance in vegetation studies within remote sensing applications (Wagner et al., 2019; Kattenborn et al., 2021). The dataset is divided into training and evaluation sets to assess the model's generalization capability. Issues can arise when creating the training and evaluation sets with a random sampling (Kattenborn et al., 2022; Ploton et al., 2020). To provide a geographically independent validation set, we define two distinct geographical regions. During the training phase, 10,000 patches of size 512 × 512 pixels with seven bands are randomly extracted from the training area for each epoch. The model produces a 1 × 512 × 512 prediction array of RH98. The mean squared error loss is computed for the pixels that have a value in the output GEDI patch. The loss is summed for each batch of data during training, and the Adam optimizer (Kingma and Ba, 2014) is applied to update the model parameters. The final model is selected as the one with the lowest loss on the validation data from the same year (occurring after 230 epochs). To create the final maps, the trained model is applied over the 2019–2020 data (partially used in training) and on the 2021–2022 data (not used in training). The predicted height map at 10 m resolution are computed per patch of 1536*1536 pixels, including an overlap area of 512 pixels from the neighboring patches to limit model field of view artifacts in the final created maps.

3 Results

3.1 Forest height maps

The produced map of top of canopy heights (RH98) detects patterns of forests height variations across the state, Figure 1.

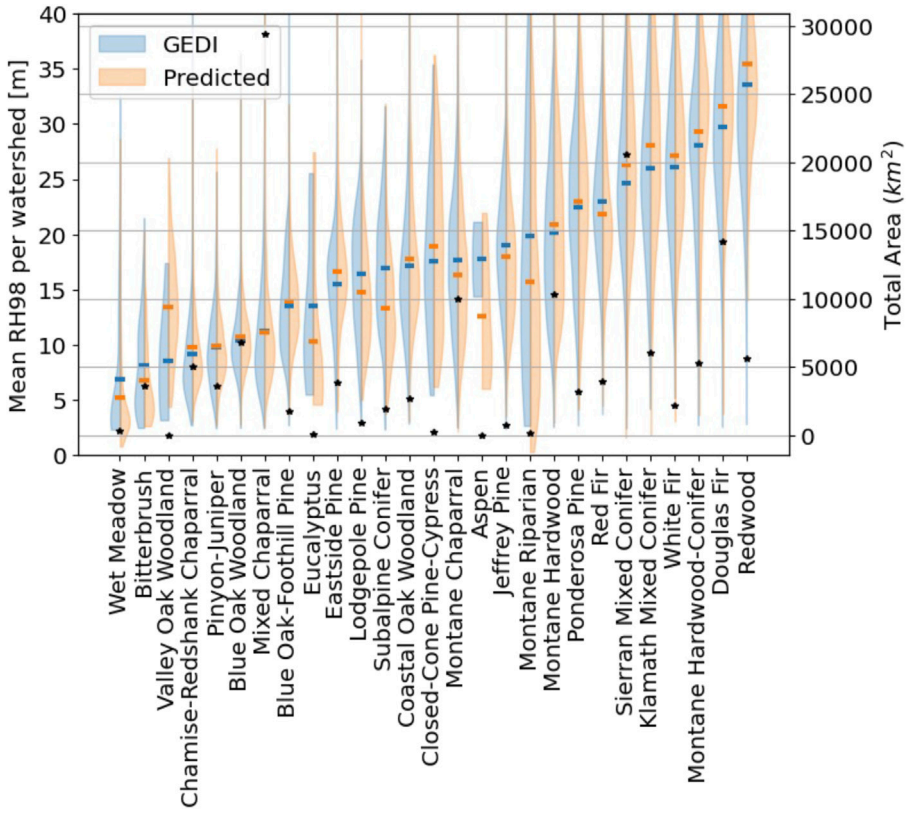

FIGURE 2
Variations of average top canopy height for California major vegetation types grouped by watershed, the violin plot shows the mean and distribution for all watersheds with a common dominant vegetation type, from GEDI samples (blue) and predicted by the model (orange), the total watershed area of each vegetation type is shown in the secondary axis (black dots).

Showing high mean top canopy height across the northwest coniferous forests (≥60 m) as well as in the Sierra Nevada. The coastal and Transverse Ranges mountainous areas in southern California also have large forest extents. The prediction ranges from 70 m average heights in the redwood forests or sequoia groves to chaparral vegetation cover across southern California mountains, transitioning to more shrublands and desert landscapes in the southern part of the state. The insets show the spatial patterns of forest height in zoomed-in areas for the coastal redwood forests (A), the managed forests in North East California (B), the Skagway grove in the Sequoia National Park (C). The high resolution data used as input allows the spatial prediction to accurately depict rivers and fire breaks and small clear-cut forest patches, for instance in the middle of the managed forests (B). The predicted heights also show variability inside forests, as in the Sequoia National Park (C) where the grove with the highest height is distinct from the dense forest cover around it.

The heights from GEDI and the model prediction are aggregated for individual watersheds across California. By area, watershed with at least one GEDI observation cover more than 50% of the total state area. The average density of 10 m pixels with a GEDI value in these watersheds is ~170 $pixel/km^2$. Figure 2 shows the variability of height across predominant vegetation types and the similarity between our estimated heights and the GEDI observed heights. For each vegetation type, we plot the mean and distribution of the watershed averaged top of canopy height, both derived from the GEDI observed data and the model's predicted map. We also estimate the area of each dominant vegetation type. Notably, watersheds dominated by redwoods exhibit an average mean top of canopy height approaching 35 m. However, disparities in average height are observable for certain vegetation types (e.g., Aspen, Eucalyptus). Such disparities can be due to the small area of these watersheds, which limits GEDI sampling, leading to large variability.

3.2 Machine learning model performance

The model reached a root mean squared error of 7.1 m on the training set and 4.46 m on the GEDI data validation set. The relative root-mean-square error, and the explained variance between the GEDI pixel values and the predicted values for the training (validation) area are respectively, 43% (56%), 0.74 (0.68) for 2019–2020 and 44% (51%), 0.73 (0.63) for 2021-2022.

The highest explained variance and the lowest RMSE are obtained with the 2019–2020 data used in training by a very slight margin. The generalization of the model is good across time, as all the metrics are consistent between the different data splits. The model generalization across the unseen validation area is slightly lower than other the same area in a different year.

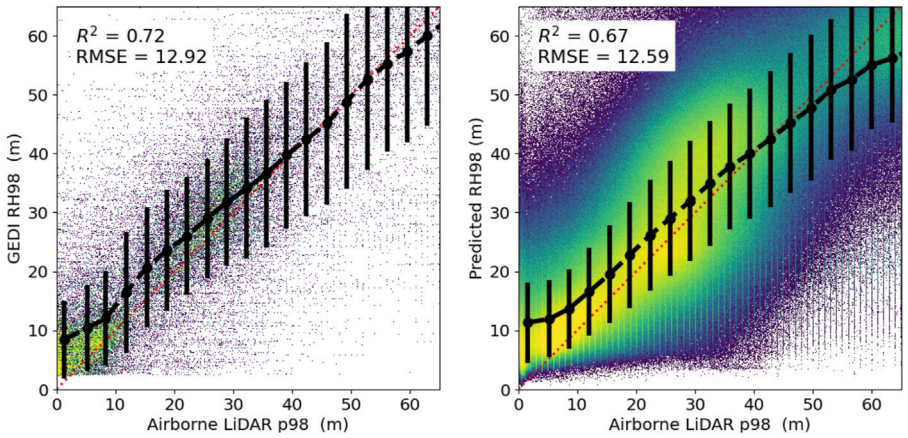

FIGURE 3
Pixel level comparison between GEDI measurements (first column) and model-predicted (second column) height metrics and the 98th percentile (first row) of ALS data across all the validation sites. Points are colored following the increasing density of pixels from blue to yellow, the mean and standard deviation of the y-axis variable within bins of the x-axis variable is shown in black, the red dotted line shows the 1:1 line.

To further analyze the model error in representing variations of GEDI RH98, we compute the residuals between the model prediction and the observed GEDI RH98 values in 2021–2022. Supplementary Figure S2 shows the absolute and relative residuals for bins in predicted height. The absolute error is ≤6 m up to 20 m height. The relative error is less than 30% for predictions ≥20 m. In addition, we look at the impact of elevation and slopes on the relative residuals, and although elevation is not associated to increase in error, slopes above 40° show a large increase in error.

3.3 Validation of spatial patterns on airborne LiDAR acquisitions

To further analyze the height predictions, we compare the predicted heights from 2019 to 2020 to the ones measured from ALS in prior years (up to 3 years prior). Figure 3 shows the comparison between the ALS data described in Section 2.2 and the predicted map for 2019–2020. The range of height values from GEDI observations and the predicted map is similar to the ALS height metrics, showing a range of top of canopy height from 0 to 60 m. Measured GEDI RH98 is in good agreement with the ALS top of canopy height across California (R^2 = 0.72). The sampling provided by GEDI is on average correct, as shown by the black line closely following the 1:1 red line. However, we observe that the error can be very large for individual pixel values, depicted by the sparse points away from the 1:1 line. This leads to a large standard deviation of GEDI derived metric for each height bin in the ALS data. This can be explained by the original ~25 m resolution of the GEDI observations, larger than the 10 m resolution at which the comparison is made. A similarly good agreement is found between the predicted height and the ALS reference, with an RMSE = 12.59 m and R^2 = 0.67 for the top of canopy height. Looking at the average binned prediction value, the figures show that both the model and GEDI height measurements do not have significant systematic errors compared to ALS data over the range of values considered. The model predictions underestimate height of very tall trees (≥ 50 m), and overestimates height of short trees (≤10 m). Similar patterns also appear when comparing GEDI and ALS data, with an overestimation of trees ≤10 m.

The spatial patterns of height variability are similar between the predicted height maps and the observed ALS for all the different vegetation types across the sites (Figure 4). The difference between the predicted and reference height in the third column highlights the overestimation of the low values (especially for the SJER site) and some discrepancies in high vegetation, as in the northern part of the SOAP site.

3.4 Monitoring forest height

The top of canopy height difference (ΔRH98) map shows the decrease in height between prediction from the 2019–2020 data to the 2021–2022, highlighting large areas affected by disturbances (high values) and low values across dense undisturbed forest areas (Figure 5). Height changes associated with timber harvests and forest management systems can also be detected by our high resolution height maps (inset A). The clear-cut forest patches are very distinct on the predicted map. The fires' delineation from CALFire is shown in green on Figure 5, where the high height difference values are mostly contained within the fire boundaries. Fires have different impacts on the landscape, and the entire fire perimeter is not necessarily strongly affected. Some very destructive fires such as the *Slater* fire in Northern California (B) removed most of the vegetation cover, the fire effect can also be more heterogeneous across the landscape such as in the *August Complex* fire. Finally, for fires affecting very low vegetation cover, as in the shrublands and desert ecosystems, the change in vegetation height might not be significant enough to be detected by this method. The average ΔRH98 can be up to ~8 m for destructive fires but varies considerably given the time to containment, area and vegetation type (Supplementary Figure S4). Some pixels show slight height increase (<2 m) between the two time periods. These

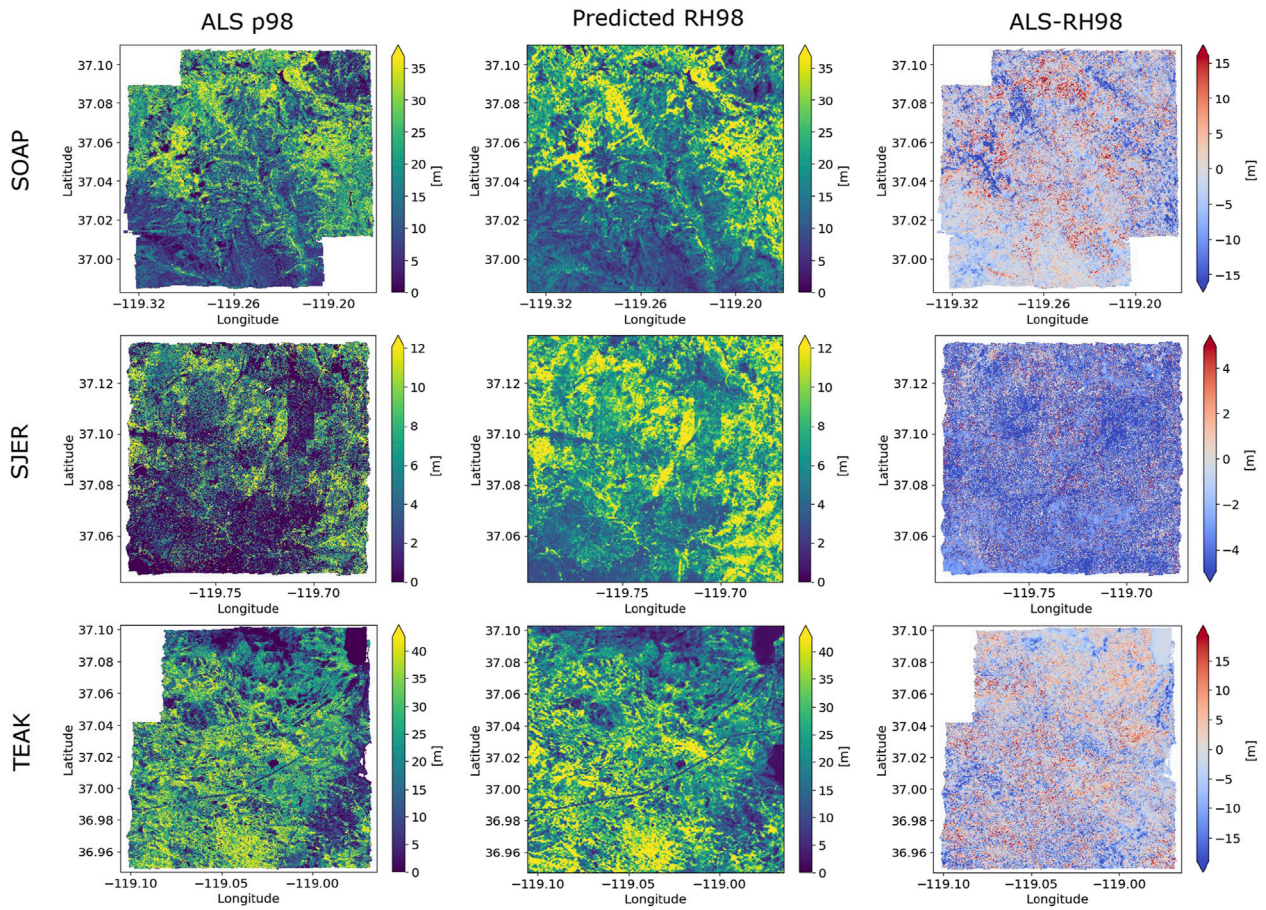

FIGURE 4
Maps of the model prediction of RH98 and ALS 98th percentile for the three NEON sites (top to bottom SOAP, SJER, TEAK) used for validation, the first column shows the ALS, the second the predicted value and the third one the difference between the first two columns.

small values were not considered for analysis being too small compared to the GEDI measurement uncertainty and model error.

The change of top of canopy height is further analyzed for fires in 2020 and 2021, and compared to the Monitoring Trends In Burn Severity (MTBS) maps output. Figure 6 shows the change of height for each class in the burn severity classification. The larger decrease in height for the increasing severity is clearly apparent. With on average ~10 m decrease in height for high severity burned areas. The severity index is derived from thresholds applied to differences of Normalized Burn Ratio. The extents align well with the ones mapped by our method but with a coarser description of the burn intensity. The range predicted height change in burned area with low severity is compatible with the uncertainty range analyzed in Section 3.2, $\sim 6\,m$.

To analyze the agreement between the predicted change and the one measured by GEDI sampling, Supplementary Figure S5 shows the change from the GEDI data averaged at the watershed level. The very sparse nature of the GEDI data makes the analysis at high resolution impossible, as there are very few pixels with repeated observations. However, it is possible to find watersheds with repeated observations and at least 100 pixels with values per square kilometer. The analysis of these repeatedly observed watersheds shows a good agreement between the change in height at the watershed level measured from GEDI and from the maps produced (Supplementary Figure S5, upper right). The largest changes in fire affected areas show up to ~20 m decrease in average height in some watersheds.

Overall, we computed the total area with more than 10 m top of canopy height in 2019-2020 whose height decreased by more than 30% in 2021-2022, and found that 8,874 km^2 of forest loss occurred in fire areas and 5,001 km^2 (~30%) occurred outside of fire affected areas, likely caused by die off and harvests. The average height loss caused by fires to the forests (RH98 ≥ 10 m) inside the fire polygons is 6.2 m.

4 Discussion

4.1 Model of canopy height based on GEDI in California

In California, our model mapped the top of canopy height for two different time periods with an explained variance of about 0.7. This shows the performance of our methodology to predict canopy heights across time and over a large range of values, up to 70 m in

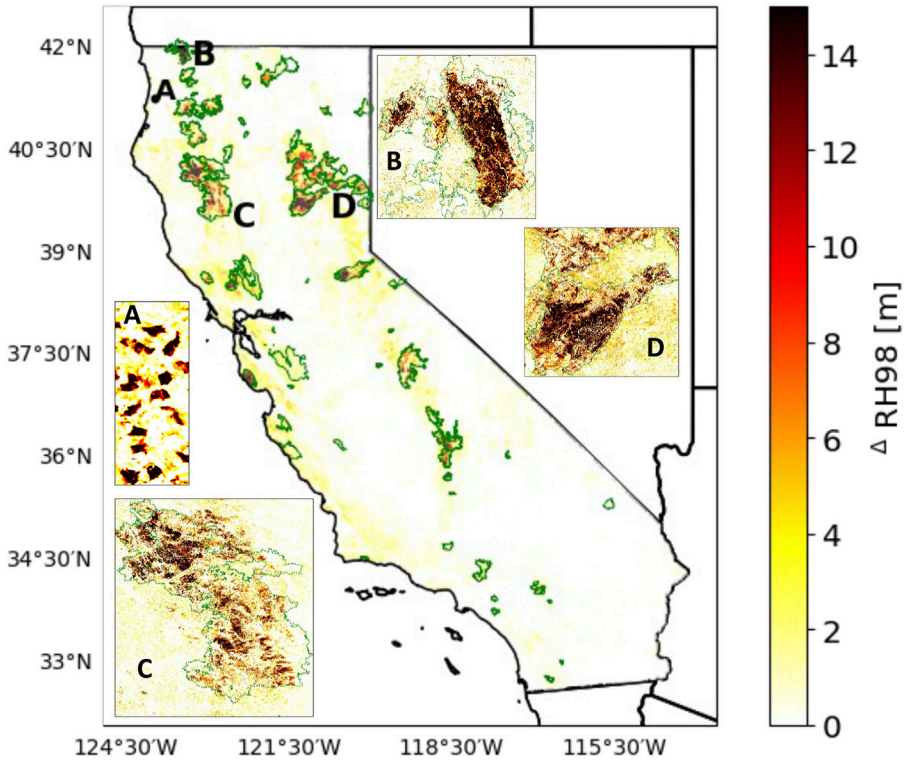

FIGURE 5
Decrease of canopy height between the 2019–2020 and the 2021–2022 period in the predicted RH98, on the global map at the watershed level and in the insets at the pixel level for a managed area in North-West California **(A)**, the *Slater* **(B)**, *August Complex* **(C)**, and *North Complex* **(D)** fires, the area delineated in green show the extents of the large fires in California that occurred in 2020 or 2021.

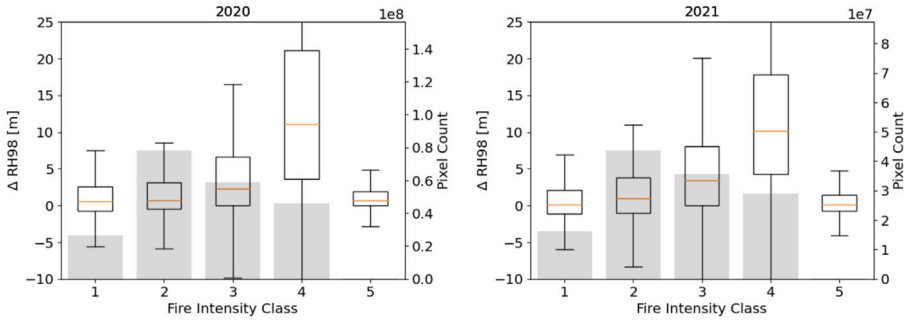

FIGURE 6
Boxplots of the mean height and interquartile range (rectangle) change between the two predicted RH98 maps for the MTBS maps for the 2020 (left) and 2021 (right) fires within each severity class (1–4 increasing burn intensity, 5 - increasing greenness post fire), the secondary axis shows the number of pixels in each class.

redwood forests. Multiple studies have attempted to derive canopy height from remote sensing predictors (Potapov et al., 2021; Lang et al., 2022) at the pixel level or using scene level features with deep learning. All models face challenges to represent the full range of vegetation heights in different parts of the world. This limited sensitivity can be explained by multiple factors: (1) the lack of information in the underlying satellite imagery (optical or radar) to predict height variations in forests. (2) The rare occurrence of very tall trees: in California, only ~1% of the land cover has a ≥50 m canopy height (Supplementary Figure S3). (3) All machine learning models face limitations predicting the extremes in the range of target values (Boucher and Aires, 2023).

The global models employ different strategies such as training data rebalancing, or model localization to alleviate the lack of sensitivity to variation of height in different regions. This study shows how a locally trained model (e.g., at the state level), helps improve the predictions compared to global approaches as shown by the reduction in RMSE (≥1 m) and increased correlation with the

ALS data (Supplementary Table S1), and by the agreement with GEDI state level distribution (Supplementary Figure S3). Alternative improvements can come by using additional information for instance from other frequencies, more sensitive to the integrated vegetation structure or higher resolution data.

A second challenge faced by remote sensing derived height maps is to achieve the highest spatial resolution possible. The effective resolution of the output maps is coarser than the 10 m resolution of Sentinel-2 observations. Different factors can explain this apparent decrease in resolution. First, the large footprint (~25 m) and possible geolocation inaccuracies from GEDI measurement cause the target variable to not represent accurately the height variations at 10 m resolution. Second, the inclusion of lower resolution predictors (DEM and radar), might not have a sufficient resolution to predict high resolution variations. Third, using convolutional layers in the encoder-decoder architecture tends to smooth structures in the predicted output map (He et al., 2022). However, it is relevant to use the highest resolution possible for the input data as it gives the model an opportunity to use all the information available. This can help improve the accuracy in some conditions, for instance to represent sparse trees outside forests, or to represent the highest vegetation structures which tend to be smoothed out at lower resolution.

Multi-temporal monitoring of heights requires precise and accurate estimations of vegetation height on different time steps. Although the results agree well with the distribution of heights measured by GEDI, the remaining uncertainties are still too large to accurately estimate growth of different forest types. In addition to the model uncertainties, the measurements available from GEDI have large uncertainties, Figure 3 and overestimate vegetation heights $\leq$10 m (Dhargay et al., 2022; Adam et al., 2020). This GEDI measurement uncertainty may limit its usability to accurately estimate small variations of vegetation height, especially in low vegetation and over short timespans. Combining the high accuracy and high resolution of ALS with the systematic sampling of GEDI could be a way to improve these estimations.

The current results already provide valuable information for decision makers. They can be used as tools to improve assessment of damages following fires, or integrated in existing fire probability models (Faivre et al., 2014; Li and Banerjee, 2021). Regarding the impact of wildfires on the Californian forests, we find that about 8,874 km^2 (60%) of forests ($\geq$10 m) height decreased by more than 30%. (Wang et al., 2022) estimated the loss of tree cover due to fires in 2020 and 2021 to be 15,760 km^2. Furthermore, the data used in this study may show a partial picture of the changes of structure caused by disturbance events. GEDI waveform profiles are more related to leaf distribution than to woody vegetation in forests. Therefore, changes measured in the fire affected areas average height, might not translate directly in variations in above ground biomass. Standing trees after fires will remain large carbon stocks, even though their height observed from LiDAR will have largely decreased. For the estimation of carbon stocks and fluxes, estimation of live and dead standing biomass requires additional work. An alternative way could be to estimate the GEDI L4A shot level biomass to directly retrieve pixel level biomass changes from different years. Overall, the agreement between studies confirms the fact that more than 60% of forest loss in California can be attributed to fires between 2019–2020 and 2021–2022. This should help target conservation and restoration efforts at the state level.

5 Conclusion

In this paper, we show how remote sensing observations and sparse GEDI LiDAR observations can be used to create a wall-to-wall maps of vegetation structure in California. A deep learning model is trained using ALOS2-PALSAR mosaics and Sentinel-2 data from the 2019–2020 period to estimate the 98th percentile (RH98) of the GEDI waveform return. The model robustness is also evaluated on the 2021–2022 period, with similar performance. It can therefore be applied to create maps on two separate dates and measure changes in vegetation height caused by degradation. The changes estimated by our method have a very good agreement with existing fire areas in California and provide a finer understanding of the degradation severity at high resolution compared to existing fire intensity maps. We find that between those years, more than 60% of forest (RH98 $\geq$ 10 m) degradation ($\geq$30% decrease in height) were caused by fires. This is key knowledge aligned with stakeholders requirements for fire life cycle understanding, from fuel mapping before fires to assessing burned areas extent and severity. Overall, this study demonstrates the benefit of the combined sparse LiDAR and other dense remote sensing products for forest monitoring at large scales and the reliability of the empirical models to derive robust change maps.

Data availability statement

The raw data used in this study are available from the original data providers. Derived products supporting the conclusions of this article will be made available by the authors upon reasonable request and without undue restrictions.

Author contributions

SF: Conceptualization, Data curation, Formal Analysis, Investigation, Methodology, Software, Validation, Visualization, Writing–original draft, Writing–review and editing, Resources. JL: Methodology, Software, Writing–review and editing. YY: Formal Analysis, Investigation, Writing–review and editing. RD: Investigation, Validation, Writing–review and editing. FW: Data curation, Supervision, Validation, Writing–review and editing. LS: Conceptualization, Investigation, Methodology, Writing–review and editing. SS: Funding acquisition, Investigation, Project administration, Resources, Supervision, Validation, Writing–review and editing.

Funding

The author(s) declare that financial support was received for the research, authorship, and/or publication of this article. Research was carried out at the Jet Propulsion Laboratory, California Institute of Technology, under a contract (19-ACCESS19-0066) with the National Aeronautics and Space Administration.

Conflict of interest

The authors declare that the research was conducted in the absence of any commercial or financial relationships that could be construed as a potential conflict of interest.

Publisher's note

All claims expressed in this article are solely those of the authors and do not necessarily represent those of their affiliated organizations, or those of the publisher, the editors and the reviewers. Any product that may be evaluated in this article, or claim that may be made by its manufacturer, is not guaranteed or endorsed by the publisher.

Supplementary material

The Supplementary Material for this article can be found online at: https://www.frontiersin.org/articles/10.3389/frsen.2024.1459524/full#supplementary-material

References

Adam, M., Urbazaev, M., Dubois, C., and Schmullius, C. (2020). Accuracy assessment of gedi terrain elevation and canopy height estimates in european temperate forests: influence of environmental and acquisition parameters. *Remote Sens.* 12, 3948. doi:10.3390/rs12233948

Anderson, M. C., Norman, J. M., Kustas, W. P., Li, F., Prueger, J. H., and Mecikalski, J. R. (2005). Effects of vegetation clumping on two–source model estimates of surface energy fluxes from an agricultural landscape during smacex. *J. Hydrometeorol.* 6, 892–909. doi:10.1175/jhm465.1

Asner, G. P., and Mascaro, J. (2014). Mapping tropical forest carbon: calibrating plot estimates to a simple lidar metric. *Remote Sens. Environ.* 140, 614–624. doi:10.1016/j.rse.2013.09.023

Badgley, G., Freeman, J., Hamman, J. J., Haya, B., Trugman, A. T., Anderegg, W. R., et al. (2022). Systematic over-crediting in California's forest carbon offsets program. *Glob. Change Biol.* 28, 1433–1445. doi:10.1111/gcb.15943

Boucher, E., and Aires, F. (2023). Improving remote sensing of extreme events with machine learning: land surface temperature retrievals from iasi observations. *Environ. Res. Lett.* 18, 024025. doi:10.1088/1748-9326/acb3e3

Bruening, J. M., May, P. B., Armston, J. D., and Dubayah, R. O. (2023). Precise and unbiased biomass estimation from gedi data and the us forest inventory. *Front. For. Glob. Change* 6, 1149153. doi:10.3389/ffgc.2023.1149153

CALVEG and California Wildlife Habitat Relationship (CWHR) (2022). *California integrated assessment of watershed health*. USFS, CA.gov: USDA.

Coffield, S. R., Vo, C. D., Wang, J. A., Badgley, G., Goulden, M. L., Cullenward, D., et al. (2022). Using remote sensing to quantify the additional climate benefits of California forest carbon offset projects. *Glob. Change Biol.* 28, 6789–6806. doi:10.1111/gcb.16380

Critchfield, W. B. (1971). *Profiles of California vegetation*, 76. Pacific Southwest Research Station.

Dalagnol, R., Wagner, F. H., Galvão, L. S., Streher, A. S., Phillips, O. L., Gloor, E., et al. (2021). Large-scale variations in the dynamics of amazon forest canopy gaps from airborne lidar data and opportunities for tree mortality estimates. *Sci. Rep.* 11, 1388. doi:10.1038/s41598-020-80809-w

CALFIRE (2023). *California fire perimeters*.

Dhargay, S., Lyell, C. S., Brown, T. P., Inbar, A., Sheridan, G. J., and Lane, P. N. (2022). Performance of gedi space-borne lidar for quantifying structural variation in the temperate forests of south-eastern Australia. *Remote Sens.* 14, 3615. doi:10.3390/rs14153615

Domke, G. M., Oswalt, S. N., Walters, B. F., and Morin, R. S. (2020) "Tree planting has the potential to increase carbon sequestration capacity of forests in the United States. *Proc. Natl. Acad. Sci. U. S. A.* 117, 24649–24651. doi:10.1073/pnas.2010840117

Dong, P., and Chen, Q. (2017). *LiDAR remote sensing and applications*. Boca Raton: CRC Press.

Drusch, M., Del Bello, U., Carlier, S., Colin, O., Fernandez, V., Gascon, F., et al. (2012). Sentinel-2: esa's optical high-resolution mission for gmes operational services. *Remote Sens. Environ.* 120, 25–36. doi:10.1016/j.rse.2011.11.026

Dubayah, R., Blair, J. B., Goetz, S., Fatoyinbo, L., Hansen, M., Healey, S., et al. (2020). The global ecosystem dynamics investigation: high-resolution laser ranging of the earth's forests and topography. *Sci. remote Sens.* 1, 100002. doi:10.1016/j.srs.2020.100002

Dubayah, R. O., and Drake, J. B. (2000). Lidar remote sensing for forestry. *J. For.* 98, 44–46. doi:10.1093/jof/98.6.44

Eitel, J. U., Höfle, B., Vierling, L. A., Abellán, A., Asner, G. P., Deems, J. S., et al. (2016). Beyond 3-d: the new spectrum of lidar applications for earth and ecological sciences. *Remote Sens. Environ.* 186, 372–392. doi:10.1016/j.rse.2016.08.018

Fahrland, E., Jacob, P., Schrader, H., and Kahabka, H. (2020). "Copernicus dem product handbook," in *Airbus defence and space*.

Faivre, N., Jin, Y., Goulden, M. L., and Randerson, J. T. (2014). Controls on the spatial pattern of wildfire ignitions in southern California. *Int. J. Wildland Fire* 23, 799–811. doi:10.1071/wf13136

Fayad, I., Ciais, P., Schwartz, M., Wigneron, J.-P., Baghdadi, N., de Truchis, A., et al. (2024). Hy-tec: a hybrid vision transformer model for high-resolution and large-scale mapping of canopy height. *Remote Sens. Environ.* 302, 113945. doi:10.1016/j.rse.2023.113945

Ferraz, A., Saatchi, S., Mallet, C., and Meyer, V. (2016). Lidar detection of individual tree size in tropical forests. *Remote Sens. Environ.* 183, 318–333. doi:10.1016/j.rse.2016.05.028

Finco, M., Quayle, B., Zhang, Y., Lecker, J., Megown, K. A., and Brewer, C. K. (2012). Monitoring trends and burn severity (mtbs): monitoring wildfire activity for the past quarter century using landsat data. *Mov. status trends For. Inventory Analysis (FIA) symposium* 2012, 4–6.

Garcia, M., Saatchi, S., Casas, A., Koltunov, A., Ustin, S., Ramirez, C., et al. (2017). Quantifying biomass consumption and carbon release from the California rim fire by integrating airborne lidar and landsat oli data. *J. Geophys. Res. Biogeosciences* 122, 340–353. doi:10.1002/2015jg003315

García, M., Saatchi, S., Casas, A., Koltunov, A., Ustin, S. L., Ramirez, C., et al. (2017). Extrapolating forest canopy fuel properties in the California rim fire by combining airborne lidar and landsat oli data. *Remote Sens.* 9, 394. doi:10.3390/rs9040394

Gorelick, N., Hancher, M., Dixon, M., Ilyushchenko, S., Thau, D., and Moore, R. (2017). Google earth engine: planetary-scale geospatial analysis for everyone. *Remote Sens. Environ.* 202, 18–27. doi:10.1016/j.rse.2017.06.031

Hakkenberg, C. R., Tang, H., Burns, P., and Goetz, S. J. (2023). Canopy structure from space using gedi lidar. *Front. Ecol. Environ.* 21, 55–56. doi:10.1002/fee.2585

He, S., Xue, H., Cheng, J., Wang, L., Wang, Y., and Zhang, Y. (2022). Tackling the over-smoothing problem of cnn-based hyperspectral image classification. *J. Appl. Remote Sens.* 16. doi:10.1117/1.jrs.16.048506

Hill, A. P., and Field, C. B. (2021). Forest fires and climate-induced tree range shifts in the western us. *Nat. Commun.* 12, 6583. doi:10.1038/s41467-021-26838-z

Jeronimo, S. M., Kane, V. R., Churchill, D. J., McGaughey, R. J., and Franklin, J. F. (2018). Applying lidar individual tree detection to management of structurally diverse forest landscapes. *J. For.* 116, 336–346. doi:10.1093/jofore/fvy023

Jucker, T. (2022). Deciphering the fingerprint of disturbance on the three-dimensional structure of the world's forests. *New Phytol.* 233, 612–617. doi:10.1111/nph.17729

Kattenborn, T., Leitloff, J., Schiefer, F., and Hinz, S. (2021). Review on convolutional neural networks (cnn) in vegetation remote sensing. *ISPRS J. Photogrammetry Remote Sens.* 173, 24–49. doi:10.1016/j.isprsjprs.2020.12.010

Kattenborn, T., Schiefer, F., Frey, J., Feilhauer, H., Mahecha, M. D., and Dormann, C. F. (2022). Spatially autocorrelated training and validation samples inflate performance assessment of convolutional neural networks. *ISPRS Open J. Photogrammetry Remote Sens.* 5, 100018. doi:10.1016/j.ophoto.2022.100018

Keane, R. E. (2002). *Cascading effects of fire exclusion in rocky mountain ecosystems: a literature review*

Keane, R. E., Cary, G. J., Davies, I. D., Flannigan, M. D., Gardner, R. H., Lavorel, S., et al. (2004). A classification of landscape fire succession models: spatial simulations of fire and vegetation dynamics. *Ecol. Model.* 179, 3–27. doi:10.1016/j.ecolmodel.2004.03.015

Kellner, J. R., Armston, J., Birrer, M., Cushman, K., Duncanson, L., Eck, C., et al. (2019). New opportunities for forest remote sensing through ultra-high-density drone lidar. *Surv. Geophys.* 40, 959–977. doi:10.1007/s10712-019-09529-9

Kellner, J. R., and Asner, G. P. (2009). Convergent structural responses of tropical forests to diverse disturbance regimes. *Ecol. Lett.* 12, 887–897. doi:10.1111/j.1461-0248.2009.01345.x

Kelly, M., Su, Y., Di Tommaso, S., Fry, D. L., Collins, B. M., Stephens, S. L., et al. (2017). Impact of error in lidar-derived canopy height and canopy base height on modeled wildfire behavior in the sierra Nevada, California, USA. *Remote Sens.* 10, 10. doi:10.3390/rs10010010

Khalefa, E., Smit, I. P., Nickless, A., Archibald, S., Comber, A., and Balzter, H. (2013). Retrieval of savanna vegetation canopy height from icesat-glas spaceborne lidar with terrain correction. *IEEE Geoscience Remote Sens. Lett.* 10, 1439–1443. doi:10.1109/lgrs.2013.2259793

Kingma, D. P., and Ba, J. (2014). Adam: a method for stochastic optimization. *arXiv Prepr. arXiv:1412.6980*. doi:10.48550/arXiv.1412.6980

Kramer, H. A., Collins, B. M., Lake, F. K., Jakubowski, M. K., Stephens, S. L., and Kelly, M. (2016). Estimating ladder fuels: a new approach combining field photography with lidar. *Remote Sens.* 8, 766. doi:10.3390/rs8090766

Lang, N., Jetz, W., Schindler, K., and Wegner, J. D. (2022). *A high-resolution canopy height model of the earth*

LaRue, E. A., Downing, A. G., Saucedo, S., Rocha, A., Zesati, S. A. V., Mata-Silva, V., et al. (2023). Diversity–volume relationships: adding structural arrangement and volume to species–area relationships across forest macrosystems. *Ecography* 2023, e06723. doi:10.1111/ecog.06723

Lefsky, M. A. (2010). A global forest canopy height map from the moderate resolution imaging spectroradiometer and the geoscience laser altimeter system. *Geophys. Res. Lett.* 37. doi:10.1029/2010gl043622

Li, S., and Banerjee, T. (2021). Spatial and temporal pattern of wildfires in California from 2000 to 2019. *Sci. Rep.* 11, 8779. doi:10.1038/s41598-021-88131-9

Lim, K. S., and Treitz, P. M. (2004). Estimation of above ground forest biomass from airborne discrete return laser scanner data using canopy-based quantile estimators. *Scand. J. For. Res.* 19, 558–570. doi:10.1080/02827580410019490

Mayer, K. E., and Laudenslayer, W. F. (1988). *A guide to wildlife habitats of California (The Department)*

McIntyre, P. J., Thorne, J. H., Dolanc, C. R., Flint, A. L., Flint, L. E., Kelly, M., et al. (2015). Twentieth-century shifts in forest structure in California: denser forests, smaller trees, and increased dominance of oaks. *Proc. Natl. Acad. Sci. U. S. A.* 112, 1458–1463. doi:10.1073/pnas.1410186112

Meyer, V., Saatchi, S., Chave, J., Dalling, J., Bohlman, S., Fricker, G., et al. (2013). Detecting tropical forest biomass dynamics from repeated airborne lidar measurements. *Biogeosciences* 10, 5421–5438. doi:10.5194/bg-10-5421-2013

Moura, Y. M. d., Balzter, H., Galvão, L. S., Dalagnol, R., Espírito-Santo, F., Santos, E. G., et al. (2020). Carbon dynamics in a human-modified tropical forest: a case study using multi-temporal lidar data. *Remote Sens.* 12, 430. doi:10.3390/rs12030430

Næsset, E. (2002). Predicting forest stand characteristics with airborne scanning laser using a practical two-stage procedure and field data. *Remote Sens. Environ.* 80, 88–99. doi:10.1016/s0034-4257(01)00290-5

National Ecological Observatory Network (NEON) (2023). *Discrete return lidar point cloud*. doi:10.48443/XXBY-5A18

Ploton, P., Mortier, F., Réjou-Méchain, M., Barbier, N., Picard, N., Rossi, V., et al. (2020). Spatial validation reveals poor predictive performance of large-scale ecological mapping models. *Nat. Commun.* 11, 4540. doi:10.1038/s41467-020-18321-y

Potapov, P., Li, X., Hernandez-Serna, A., Tyukavina, A., Hansen, M. C., Kommareddy, A., et al. (2021). Mapping global forest canopy height through integration of gedi and landsat data. *Remote Sens. Environ.* 253, 112165. doi:10.1016/j.rse.2020.112165

Pugh, T. A., Lindeskog, M., Smith, B., Poulter, B., Arneth, A., Haverd, V., et al. (2019). Role of forest regrowth in global carbon sink dynamics. *Proc. Natl. Acad. Sci.* 116, 4382–4387. doi:10.1073/pnas.1810512116

Quirion, B. R., Domke, G. M., Walters, B. F., Lovett, G. M., Fargione, J. E., Greenwood, L., et al. (2021). Insect and disease disturbances correlate with reduced carbon sequestration in forests of the contiguous United States. *Front. For. Glob. Change* 4, 716582. doi:10.3389/ffgc.2021.716582

Ronneberger, O., Fischer, P., and Brox, T. (2015) "U-net: convolutional networks for biomedical image segmentation," in *Medical image computing and computer-assisted intervention–MICCAI 2015: 18th international conference, Munich, Germany, october 5-9, 2015, proceedings, Part III*, 18. Springer International Publishing.

Rosenqvist, A., Shimada, M., Ito, N., and Watanabe, M. (2007). Alos palsar: a pathfinder mission for global-scale monitoring of the environment. *IEEE Trans. Geoscience Remote Sens.* 45, 3307–3316. doi:10.1109/tgrs.2007.901027

Roussel, J.-R., Auty, D., Coops, N. C., Tompalski, P., Goodbody, T. R., Meador, A. S., et al. (2020). lidr: an r package for analysis of airborne laser scanning (als) data. *Remote Sens. Environ.* 251, 112061. doi:10.1016/j.rse.2020.112061

Rybansky, M., Brenova, M., Cermak, J., van Genderen, J., and Sivertun, Å. (2016). Vegetation structure determination using lidar data and the forest growth parameters. *IOP Conf. Ser. Earth Environ. Sci.* 37, 012031, doi:10.1088/1755-1315/37/1/012031

Saatchi, S., Halligan, K., Despain, D. G., and Crabtree, R. L. (2007). Estimation of forest fuel load from radar remote sensing. *IEEE Trans. geoscience remote Sens.* 45, 1726–1740. doi:10.1109/tgrs.2006.887002

Saatchi, S. S., Harris, N. L., Brown, S., Lefsky, M., Mitchard, E. T., Salas, W., et al. (2011). Benchmark map of forest carbon stocks in tropical regions across three continents. *Proc. Natl. Acad. Sci.* 108, 9899–9904. doi:10.1073/pnas.1019576108

Schimel, D., Hargrove, W., Hoffman, F., and MacMahon, J. (2007). Neon: a hierarchically designed national ecological network. *Front. Ecol. Environ.* 5, 59. doi:10.1890/1540-9295(2007)5[59:nahdne]2.0.co;2

Schwartz, M., Ciais, P., De Truchis, A., Chave, J., Ottlé, C., Vega, C., et al. (2023). Forms: forest multiple source height, wood volume, and biomass maps in France at 10 to 30 m resolution based on sentinel-1, sentinel-2, and global ecosystem dynamics investigation (gedi) data with a deep learning approach. *Earth Syst. Sci. Data* 15, 4927–4945. doi:10.5194/essd-15-4927-2023

Shimada, M., Itoh, T., Motooka, T., Watanabe, M., Shiraishi, T., Thapa, R., et al. (2014). New global forest/non-forest maps from alos palsar data (2007–2010). *Remote Sens. Environ.* 155, 13–31. doi:10.1016/j.rse.2014.04.014

Skowronski, N. S., Clark, K. L., Duveneck, M., and Hom, J. (2011). Three-dimensional canopy fuel loading predicted using upward and downward sensing lidar systems. *Remote Sens. Environ.* 115, 703–714. doi:10.1016/j.rse.2010.10.012

Stark, S. C., Leitold, V., Wu, J. L., Hunter, M. O., de Castilho, C. V., Costa, F. R., et al. (2012). Amazon forest carbon dynamics predicted by profiles of canopy leaf area and light environment. *Ecol. Lett.* 15, 1406–1414. doi:10.1111/j.1461-0248.2012.01864.x

Su, Y., Ma, Q., and Guo, Q. (2017). Fine-resolution forest tree height estimation across the sierra Nevada through the integration of spaceborne lidar, airborne lidar, and optical imagery. *Int. J. Digital Earth* 10, 307–323. doi:10.1080/17538947.2016.1227380

Tan, M., and Le, Q. (2021). "Efficientnetv2: smaller models and faster training," in *International Conference on machine learning (PMLR)*.

Tang, H., Brolly, M., Zhao, F., Strahler, A. H., Schaaf, C. L., Ganguly, S., et al. (2014). Deriving and validating leaf area index (lai) at multiple spatial scales through lidar remote sensing: a case study in sierra national forest, ca. *Remote Sens. Environ.* 143, 131–141. doi:10.1016/j.rse.2013.12.007

The Cadmus Group, Inc. (2013). *California integrated assessment of watershed health. EPA Report*. U.S. Environmental Protection Agency.

Vepakomma, U., St-Onge, B., and Kneeshaw, D. (2008). Spatially explicit characterization of boreal forest gap dynamics using multi-temporal lidar data. *Remote Sens. Environ.* 112, 2326–2340. doi:10.1016/j.rse.2007.10.001

Vogeler, J. C., Fekety, P. A., Elliott, L., Swayze, N. C., Filippelli, S. K., Barry, B., et al. (2023). Evaluating gedi data fusions for continuous characterizations of forest wildlife habitat. *Front. Remote Sens.* 4, 1196554. doi:10.3389/frsen.2023.1196554

Wagner, F. H., Sanchez, A., Tarabalka, Y., Lotte, R. G., Ferreira, M. P., Aidar, M. P. M., et al. (2019). Using the u-net convolutional network to map forest types and disturbance in the atlantic rainforest with very high resolution images. *Remote Sens. Ecol. Conservation* 5, 360–375. doi:10.1002/rse2.111

Wang, J. A., Randerson, J. T., Goulden, M. L., Knight, C. A., and Battles, J. J. (2022). Losses of tree cover in California driven by increasing fire disturbance and climate stress. *AGU Adv.* 3, e2021AV000654. doi:10.1029/2021av000654

Williams, C. A., Gu, H., MacLean, R., Masek, J. G., and Collatz, G. J. (2016). Disturbance and the carbon balance of us forests: a quantitative review of impacts from harvests, fires, insects, and droughts. *Glob. Planet. Change* 143, 66–80. doi:10.1016/j.gloplacha.2016.06.002

Wulder, M. A., Bater, C. W., Coops, N. C., Hilker, T., and White, J. C. (2008). The role of lidar in sustainable forest management. *For. Chron.* 84, 807–826. doi:10.5558/tfc84807-6

Yu, Y., Saatchi, S., Domke, G. M., Walters, B., Woodall, C., Ganguly, S., et al. (2022). Making the us national forest inventory spatially contiguous and temporally consistent. *Environ. Res. Lett.* 17, 065002. doi:10.1088/1748-9326/ac6b47